Basins of attraction of a nonlinear nanomechanical resonator

I. Kozinsky[*][†] H.W.Ch. Postma[*][‡] O. Kogan, A. Husain,[§] and M.L. Roukes[¶]

Kavli Nanoscience Institute and Condensed Matter Physics 114-36,
California Institute of Technology, Pasadena, CA 91125
(Dated: February 1, 2008)

We present an experiment that systematically probes the basins of attraction of two fixed points of a nonlinear nanomechanical resonator and maps them out with high resolution. We observe a separatrix which progressively alters shape for varying drive strength and changes the relative areas of the two basins of attraction. The observed separatrix is blurred due to ambient fluctuations, including residual noise in the drive system, which cause uncertainty in the preparation of an initial state close to the separatrix. We find a good agreement between the experimentally mapped and theoretically calculated basins of attraction.

In the last few years the dimensions of mechanical devices have been scaled deep into the submicrometer regime. This decrease in size has resulted not only in the increased detection sensitivity of extremely small physical quantities, such as zeptogram-scale mass [1] and single electron spin [2], but also in an enhancement of the significance of nonlinear dynamics in such devices [3]. The growing significance of nonlinearities in high-frequency nanomechanical devices has consequences not only for fundamental studies of nonlinear dynamics, but also for advances in sensing applications. It was recently shown that precision of some experimental measurements on nanoscale can be improved by deliberately operating the system in the nonlinear regime. For example, a nonlinear resonator can be employed to suppress amplifier noise in an oscillator circuit [4], noise-induced switching between two stable states in a nonlinear beam resonator enables precision measurement of the resonant frequency [5], and the sensitivity of a resonator for mass detection can be improved when the resonator is driven into a region of nonlinear oscillations [6]. Finally, in a Josephson junction, which is dynamically similar to a mechanical resonator in nonlinear regime, the bistable state of the nonlinear system can be used as a bifurcation amplifier to perform a non-dissipative, low-back-action measurement of the phase across the junction [7]. When nanomechanical devices reach the quantum-limited regime [8], a nanomechanical version of such an amplifier could be used for a similar sensitive low-back-action measurement of the state of a quantum mechanical resonator. Nonlinear response of nanomechanical resonators could also be used to detect transition from classical to quantum regime [9, 10]. It is therefore important to understand nonlinear dynamics of these systems well, so that we can fully realize their potential in expanding our experimental capabilities.

Although some work has been done with parametric systems [11, 12], the majority of nonlinear nanoscale systems that have been studied are directly driven [5, 13, 14] and the dominant nonlinearity in the restoring force is cubic, also known as Duffing nonlinearity. When a system is driven strongly, the Duffing nonlinearity causes the resonance response curve to become asymmetric. The resonance is pulled either to the right for positive, also known as hardening, nonlinearity (e.g. geometric nonlinearity [15], Figure 1(b)) or to the left for negative, or softening, nonlinearity (e.g. nonlinearities of material [16], capacitive, or inertial [17] origins). When the resonance is pulled far enough to one side, hysteretic behavior is observed as two stable states appear in the system [18]. The stable states, known as "attractors" or "fixed points", correspond to the points in state space to which the system converges with time. For each attractor, a set of initial states that dynamically evolves to that attractor forms its basin of attraction, which is separated from the rest of the state space by the separatrix curve. The dependence of fixed points and basins of attraction on driving frequency and amplitude has been exploited for precision measurement applications mentioned earlier.

There have been very few experimental studies of basins of attraction because following the evolution of initial conditions in low-frequency macroscopic systems is usually very time-consuming and system parameters tend to drift over the course of many data-taking runs. Previous mappings of basins of attraction [19, 20] used the method of stochastic interrogation, where the system is stochastically perturbed and initial states are sampled at random without fully covering the basins.

We demonstrate the ability to systematically prepare a nonlinear, Duffing-type nanomechanical resonator in the required set of initial states and map the basins of attraction of its two fixed points with high resolution. Our experiment is enabled by the fact that the relevant time scale per data point, $\sim Q/f_0$, is very short for very-high-frequency nanometer-scale devices. This allows us to take many data points in a relatively short time with minimal drift in the parameters of the system. We also observe that the separatrix changes shape for varying drive
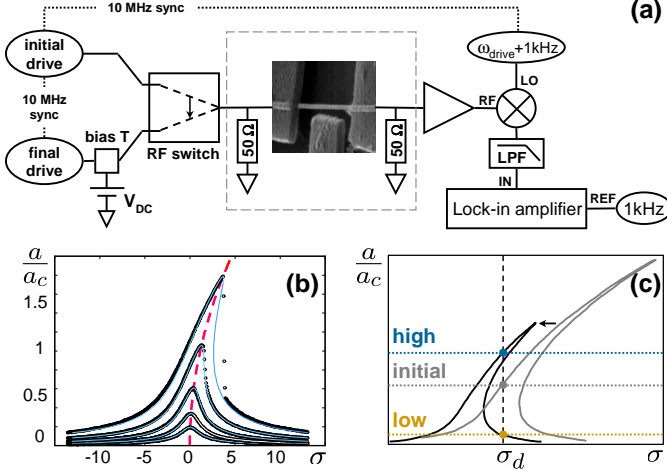
FIG. 1: **(a)** Experimental layout. The initial drive prepares an initial state of the platinum nanowire resonator (shown in the SEM photo), a 5 ns RF switch is then flipped to connect to the final drive, and the state of the device is measured by a lock-in amplifier after mixing down to a low (1 kHz) frequency and filtering the residual RF signal.
(b) Vibration amplitude versus frequency, for various driving powers at the sample (-90, -85, -80, -75, -70 dBm, or normalized to the critical drive V_c=28.4 μV, V/V_c=0.249, 0.443, 0.788, 1.401, 2.492) showing the onset of nonlinearity in the platinum nanowire resonator. We plot the response normalized to the critical amplitude, a_c, versus normalized detuning frequency $\sigma \equiv 2Q(f/f_0 - 1)$. The backbone curve (dashed line) connects the maxima of the resonance curves and follows $(a_p/a_c)^2 = \sqrt{3}\sigma/2$.
(c) The state of the nanowire resonator is first prepared in an initial state on the initial response curve (grey) by choosing an appropriate drive strength for the fixed detuning frequency, $\sigma_d = 4.26$. After the RF switch is flipped to connect the final drive, the response curve changes to the one shown in black and the initial state evolves to either the high-amplitude state or low-amplitude state. The small bias voltage, applied to the nanowire together with the final drive, is chosen so that the hysteresis loop of the initial curve is at higher frequency than the operating frequency.

strength, so that one of the basins becomes progressively smaller and eventually disappears. The mapped basins of attraction show good agreement with theory. However, the observed separatrix is blurred due to ambient fluctuations, including residual noise in the drive system, which cause uncertainty in the preparation of an initial state.

The device used for mapping the basins of attraction, a doubly-clamped platinum nanowire, is shown in the scanning electron microscope (SEM) photograph in Figure 1(a). The nanowire, with a length L of 2.25 μm and a diameter of 35 nm, is grown by electrodeposition of platinum into a nanoporous membrane [21]. Gold contact pads on both ends and a gate are fabricated using electron beam lithography, and about 150 nm of the substrate is subsequently etched away in hydrofluoric acid to

suspend the device [13]. We actuate and detect the vibration of the nanowire magnetomotively [22] in a magnetic field, $B = 8$ T, in a cooled (to about 20 K) probe in vacuum . The magnetic field is applied perpendicular to the device so that the vibration is in the plane of the gate electrode. At low driving powers the resonance curve is linear, and we extract a resonant frequency of 45.35 MHz and mechanical quality factor of 6045. The resonant frequency is higher than the expected 17.71 MHz for this device geometry, most likely due to differential thermal contraction between the silicon wafer and the gold contacts that results in residual tension. The ratio of electromechanical impedance, R_{em}, to electrical impedance, R_e, is 0.222, which indicates the presence of significant eddy current damping [23]. The quality factor corrected for the eddy current damping is $Q_0 = Q/(1 - R_{em}/R_e) = 7770$.

The resonant response of the nanowire to different drives is shown in Figure 1(b). With increasing drive power, the resonance is pulled to higher frequencies at large amplitudes, ultimately forming a hysteretic region. The nonlinearity of the device is fully characterized by the critical amplitude a_c, the point where the resonance curve develops infinite slope, $\frac{da}{df}|_{a=a_c} = -\infty$. The theoretical curves (thin solid lines) in Figure 1(b) are generated using the critical amplitude, a_c, as the only fitting parameter. We determine a_c by fitting the backbone curve that connects the peaks of resonant curves for different drives to the theoretical expression $(a_p/a_c)^2 = \sqrt{3}\sigma/2$ [24], where $\sigma \equiv 2Q(f/f_0 - 1)$ is the detuning frequency scaled by the width of the resonance and a_p is the peak amplitude. The critical amplitude value $a_c = 2.68$ nm, extracted from the experimental data in this manner, is in reasonable agreement with the value calculated for our nanowire geometry [3] when the round-trip loss in the experimental circuit is taken into account.

The dominant source of nonlinearity in doubly-clamped NEMS resonators is the additional tension in the beam that appears when vibrations are sufficiently large. This extra tension gives rise to a cubic nonlinearity in the spring constant term in the equation of motion [3], giving it a Duffing oscillator form:

$$\ddot{x} + \frac{\omega_0}{Q}\dot{x} + \omega_0^2(x + \alpha x^3) = F\cos(\Omega t). \qquad (1)$$

Here, $x(t)$ is the displacement of the beam, $\omega_0 = 2\pi f_0$ is the resonance frequency, $\alpha = 2\sqrt{3}/(9a_c^2 Q)$ is the nonlinearity parameter [24], $\Omega = 2\pi f = (\sigma/(2Q) + 1)\omega_0$ is the driving frequency, and F is the force per unit mass acting on the resonator of mass m. The driving force in the magnetomotive transduction scheme is the Lorentz force that acts on the nanowire when a current $I_d(t)$ is passed through it in a magnetic field, $F = LBI_d(t)/m$. When the driving voltage amplitude is V_d, the driving current is given by $I_d \approx V_d/R_e$.

As illustrated in Figure 1(a), we prepare the system by exciting it with an initial drive amplitude, V_i, and

then switching to a final drive amplitude, V_f. Two RF sources (HP 8648B for initial and SR DS345 with a frequency doubler for final drive) are tuned to the same fixed frequency off resonance, $\sigma_d = 4.26$. Their internal clocks and that of the local oscillator (LO) are synchronized with their 10 MHz clock reference. The phase of the final drive lags behind the initial drive phase by the phase difference ϕ. By changing ϕ while holding the initial drive amplitude, V_i, constant, we can prepare the resonator in the initial states corresponding to a circle in state space. By also stepping the initial drive values, V_i, we can cover a disk of initial states in state space. We switch rapidly from the initial to final drive using a 5 ns ($< 1/f_0 \sim 22$ ns) RF switch (Mini-Circuits ZASWA-2-50DR). After the switching occurs, we measure the final amplitude of the oscillator and mark it as a low or a high final amplitude. In order to access a continuum of initial states, we apply a small DC bias voltage of $V_{dc} \approx 10$ mV to the wire in the final state. The capacitive interaction with the gate lowers the resonant frequency of the final state [25] so that the hysteretic frequency response of the final state occurs at the same frequency as the single-valued resonant response of the initial state (Figure 1(c)). Without this technique, the resonator cannot be prepared in the initial states corresponding to the unstable branch of the initial drive resonance and an annulus of these states in state space would not be accessible in the experiment.

To map the basins of attraction in this manner, the initial states were driven with -90 to -50 dBm in 60 concentric circles with 60 phase points per circle, corresponding to a displacement range of 0 to $2.5a_c$, where a_c is the critical amplitude extracted from experimental data as shown in Figure 1(b). Each of the initial states was marked according to the attractor that it evolved to after the switch was flipped: blue for the high-amplitude state and yellow for the low-amplitude state. This data was re-rastered using a nearest neighbor search algorithm to create the continuous color plots shown in Figure 2.

For very low final drives, there is only one state the resonator can occupy (refer to Figure 1(b)). As the final drive starts exciting a nonlinear response, a second basin representing the high-amplitude stable state appears, but subtends a smaller fraction of the state space (Figure 2(1)). When the final drive amplitude is increased, the high-amplitude basin grows, and the low-amplitude basin gets progressively smaller and eventually disappears (Figure 2(6)). The disappearance of the low-amplitude state can also be observed in Figure 1(b): a large final drive results in a wider hysteretic region that moves to the right, where the low amplitude branch starts at $\sigma > \sigma_d$, so only the high-amplitude state is available to the system operating at σ_d.

In order to calculate the location of the fixed points and the separatrix in state space, we obtain the time-dependent solution $x(t)$ that describes the response of
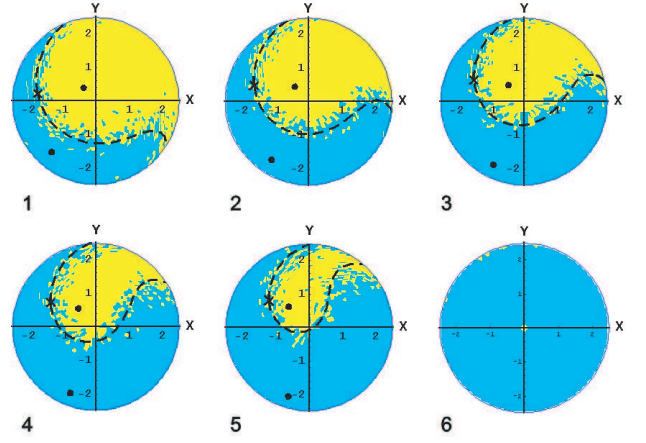

FIG. 2: Basins of attraction of a nanowire resonator at a fixed frequency, $\sigma_d = 4.26$, for increasing final drive values, $V_f/V_c = (1)1.867, (2)2.049, (3)2.237, (4)2.434, (5)2.640, (6)2.741$. Blue and yellow colors indicate the final high- and low-amplitude states, respectively. The data consists of 60 concentric circles with 60 points each, corresponding to a displacement range of 0 to $2.5a_c$. This data is converted into a continuous plot using a nearest neighbor search algorithm to fill out the space between data points. Theoretical fixed points, saddle point, and separatrix curve are indicated by black points, black cross, and the dashed black curve respectively.

the nonlinear system to a disturbance. In our devices, we can separate the dynamics described by the equation of motion (1) into two parts: the fast dynamics on a time scale of $1/\omega_0$, corresponding to the fast oscillations of the undamped harmonic version of the system; and the slow dynamics on a much longer time scale Q/ω_0, associated with a slight detuning σ of the driving frequency from resonance as well as damping and nonlinearity (method of multiple scales [24]). Then the solution to the equation of motion (1) can be written as $x_0(t,T) = A(T)e^{i\omega_0 t} + \bar{A}(T)e^{-i\omega_0 t}$, where time variable t characterizes the fast dynamics and T, the slow dynamics. The slowly varying amplitude $A(T) = (X(T) + iY(T))\exp(i\omega_0\sigma/2T)$ obeys the envelope equations:

$$\frac{\mathrm{d}X}{\mathrm{d}T} = -\frac{\omega_0 X}{2} + \frac{\sigma\omega_0}{2}Y - \frac{3\alpha Q\omega_0}{2}(X^2 + Y^2)Y \quad (2)$$
$$\frac{\mathrm{d}Y}{\mathrm{d}T} = -\frac{\omega_0 Y}{2} - \frac{\sigma\omega_0}{2}X + \frac{3\alpha Q\omega_0}{2}(X^2 + Y^2)X - \frac{FQ}{4\omega_0}.$$

We have assumed here that $1/Q \ll 1$, and the slowly-varying amplitude approximation implies that $\ddot{A}(t)$ terms are negligible compared to $\dot{A}$ terms.

The slowly-varying amplitude equations describe the nonlinear dynamics of the system and allow us to determine the location of two attracting fixed points and one metastable saddle point in state space for different values of parameters F and σ, which can be extracted from the experimental data. A set of points in state space that evolve into the saddle point defines the separatrix. To

calculate the separatrix, we evolve the initial conditions, lying close to this fixed point and along the negative-eigenvalue eigenvector (which is obtained by linearizing the above equations around the saddle fixed point), backwards in time according to the full equations (2). The curves generated by this procedure constitute the separatrix. To compare these theoretical calculations to the experimental data in Figure 2, we scale computed amplitudes by the value of the critical amplitude, a_c, calculated from equations (2).

The black points in Figure 2 are the theoretical fixed points, the black cross is the saddle point, and the dashed black curve corresponds to the theoretical calculation of the separatrix for the experimental parameters used: $\sigma_d = 4.26$, $(a/a_c)_{max} = 2.5$, and the first five final drive values scaled by critical drive, V_f/V_c, listed in the caption. We find good agreement between the experimental data and our theoretical calculations for the basins of attraction.

The separatrix observed in the experiment is blurred due to environmental noise affecting the system. The following analysis implies that most of this noise results from the voltage noise in the drive circuit. These fluctuations perturb the initial state of the resonator and so cause uncertainty in the preparation of the initial state. For the states near the separatrix, switching the system to the bistable regime and forcing the initial state to project on either of the two stable states amplifies this jitter and results in the noisy separatrix in Figure 2. In principle, the full solution for the probability distribution of the initial state of the Duffing resonator with noise would be obtained by solving the Fokker-Planck equation. Since the system is operated away from the bifurcation, the time scale on which noise affects the system is much slower than the ringdown time of the resonator and the dynamics can be analyzed in the small-noise approximation. We can then consider two scenarios for how external noise can affect the system, either additively or as parameter noise.

If noise in equations (2) for the initial state is additive, the evolution of the initial condition follows the deterministic path perturbed by small jitter until the system reaches the neighborhood of an attracting fixed point, corresponding to the initial state. The action of this noise is to perturb the system around the fixed point within a characteristic radius δa. If the additive noise in equation (1) is white with power spectral density γ, then the effective temperature of the noise in the system described by equations (2) is $\frac{\gamma \alpha Q^2}{8m^2\omega_0^3}$. From the equipartition theorem, δa is given by

$$\frac{(\delta a)^2}{a_c^2} = \left(\frac{3}{\sqrt{2}}\right)^{3/2} \frac{\gamma \alpha Q^2}{4m^2\omega_0^3}. \tag{3}$$

We can estimate the uncertainty in the preparation of the initial amplitude from the observed blurring of the

separatrix, $\delta a/a_c$, in Figure 2 to be about 10%. The force noise that would result in such blurring is 5 pN/$\sqrt{\text{Hz}}$. For the Lorentz force due to the magnetomotive drive, this force noise translates to a voltage noise of 18 nV/$\sqrt{\text{Hz}}$.

Alternatively, the noise can be present in the parameters of the system. The noise in the magnitude of the drive, F, results in the fluctuations of the position of the initial fixed point. Near the origin, where a/a_c is small, the variation in the drive voltage $\delta V/V_c$ that would cause this variation in amplitude is calculated from equations (2) to be $\delta V/V_c = (\sqrt{3}/2)a/a_c$. For the estimated blurring of the separatrix, $\delta a/a_c$, of about 10%, the variation in the drive amplitude is $\delta V/V_c = 8.7\%$. (Farther away from the origin, up to $a/a_c = 2.5$, fluctuations in the drive voltage have less effect on fluctuations in the amplitude due to nonlinear suppression.) Therefore, the observed blurring translates to fluctuations of $\delta V \approx 2.5$ μV for the measured critical drive, $V_c = 28$ μV. The relevant noise bandwidth for this resonator is $\pi f_0/Q = 24$ kHz. The noise spectrum that would account for the 10% fluctuation in amplitude is then 16 nV/$\sqrt{\text{Hz}}$. This result is consistent with the above estimate of fluctuations due to additive noise. The residual voltage noise from the initial-drive function generator and the rest of the drive circuit of about 5 μV/$\sqrt{\text{Hz}}$ is attenuated by 51 dBm by the RF switch and additional attenuators (not shown), and results in a voltage noise of 14 nV/$\sqrt{\text{Hz}}$ at the sample. The drive-circuit noise therefore accounts for most of the observed fluctuations near the separatrix.

The presence of noise can also cause transitions from one fixed point to another [26, 27]. We indeed observe the same noise-induced switching between two stable states as in References [5] and [28], where the noise from the drive source has an effect of shrinking the size of the hysteresis loop and inducing transitions of a resonator from one state to the other near the bifurcation points. By adding noise to the resonator drive and recording the statistics of the time it takes for the system to switch when it is near the bifurcation point, we find that the transition rate varies as $\exp(-E_a/\nu)$, where $\nu = k_B T_{eff}$ is the noise power and E_a is the height of the energy barrier that the system needs to overcome for the transition to happen. The energy barrier depends on the distance to the bifurcation point V_b: $E_a \sim (V - V_b)^\delta$. We have measured the critical exponent δ to be 1.8 ± 0.3, which is close to the theoretically predicted value of $3/2$ in the region we operate in [26, 27, 29]. Measurement of transitions induced by noise in the bistable regime of a nanoscale resonator could thus enable a very sensitive experimental technique to detect mechanical fluctuations.

The experimental mapping of basins of attraction of a nanowire mechanical resonator presented here fills a large gap in our understanding of nonlinear dynamics of nanoscale systems. Since the nonlinear regime is readily accessible in nanoscale devices, the details of dynamical behavior are now increasingly important for proper en-

gineering and analysis of these systems. The knowledge of basin dynamics and noise-induced transitions should also prove useful for precision measurement applications, such as nanomechanical bifurcation amplifiers [12], detection of transition to the quantum regime [9, 10], or a sensitive monitoring of intrinsic device noise processes.

[†] now at Bosch Research and Technology Center, Palo Alto, CA 94304

[‡] now at Physics and Astronomy Dept., California State University at Northridge, Northridge, CA 91330-8268

[§] now at International Rectifier, El Segundo, CA 90245

[1] Y. T. Yang, C. Callegari, X. L. Feng, K. L. Ekinci, and M. L. Roukes, Nano Letters **6**, 583 (2006).

[2] D. Rugar, R. Budakian, H. J. Mamin, and B. W. Chui, Nature **430**, 329 (2004).

[3] H. W. C. Postma, I. Kozinsky, A. Husain, and M. L. Roukes, Applied Physics Letters **86**, 223105 (2005).

[4] B. Yurke, D. S. Greywall, A. N. Pargellis, and P. A. Busch, Physical Review A **51**, 4211 (1995).

[5] J. S. Aldridge and A. N. Cleland, Physical Review Letters **94**, 156403 (2005).

[6] E. Buks and B. Yurke, Physical Review E **74**, 046619 (2006).

[7] I. Siddiqi, R. Vijay, F. Pierre, C. M. Wilson, M. Metcalfe, C. Rigetti, L. Frunzio, and M. H. Devoret, Physical Review Letters **93**, 207002 (2004).

[8] M. D. LaHaye, O. Buu, B. Camarota, and K. C. Schwab, Science **304**, 74 (2004).

[9] I. Katz, A. Retzker, R. Straub, and R. Lifshitz, Physical Review Letters **99**, 040404 (2007).

[10] V. Peano and M. Thorwart, Physical Review B **70**, 235401 (2004).

[11] A. N. Cleland, New Journal of Physics **7**, 235 (2005).

[12] R. Karabalin, R. Lifshitz, S. Masmanidis, M. Cross, and M. L. Roukes, to be published (2007).

[13] A. Husain, J. Hone, H. W. C. Postma, X. M. H. Huang, T. Drake, M. Barbic, A. Scherer, and M. L. Roukes, Applied Physics Letters **83**, 1240 (2003).

[14] A. Erbe, H. Kroemmer, A. Kraus, R. H. Blick, G. Corso, and K. Richter, Applied Physics Letters **77**, 3102 (2000).

[15] L. D. Landau and E. M. Lifshitz, *Theory of Elasticity*, vol. 7 of *Course of Theoretical Physics* (Butterworth Heinemann, Oxford, Boston, 1986), 3rd ed.

[16] V. V. Bolotin, *The Dynamic Stability of Elastic Systems*, *Holden-Day Series in Mathematical Physics* (Holden-Day, Inc., San Francisco, 1964).

[17] S. Atluri, Journal of Applied Mechanics **40**, 121 (1973).

[18] L. D. Landau and E. M. Lifshitz, *Mechanics*, vol. 1 of *Course of Theoretical Physics* (Butterworth Heinemann, Oxford, 1981), 3rd ed.

[19] J. P. Cusumano and B. W. Kimble, Nonlinear Dynamics **8**, 213 (1995).

[20] L. N. Virgin, M. D. Todd, C. J. Begley, S. T. Trickey, and E. H. Dowell, International Journal of Bifurcation and Chaos **8**, 521 (1998).

[21] C. R. Martin, Science **266**, 1961 (1994).

[22] A. N. Cleland and M. L. Roukes, Sensors and Actuators A **72**, 256 (1999).

[23] K. Schwab, Applied Physics Letters **80**, 1276 (2002).

[24] A. H. Nayfeh and D. T. Mook, *Nonlinear Oscillations*, *Physics and Applied Mathematics: A Wiley-Interscience Series of Texts, Monographs & Tracts* (John Wiley & Sons, New York, 1979), 1st ed.

[25] I. Kozinsky, H. W. C. Postma, I. Bargatin, and M. L. Roukes, Applied Physics Letters **88**, 253101 (2006).

[26] J. Kurkijarvi, Physical Review B **6**, 832 (1972).

[27] M. I. Dykman and M. A. Krivoglaz, Soviet Physics JETP **50**, 30 (1979).

[28] C. Stambaugh and H. B. Chan, Physical Review B **73**, 172302 (2006).

[29] O. Kogan and M. I. Dykman, manuscript in preparation (2007).